The Crystal Structure of Eosinophil Cationic Protein in Complex with 2′,5′-ADP at 2.0 Å Resolution Reveals the Details of the Ribonucleolytic Active Site[†,‡]

C. Gopi Mohan,[§] Ester Boix,[§,||] Hazel R. Evans,[§] Zoran Nikolovski,[||] M. Victòria Nogués,[||] Claudi M. Cuchillo,[||] and K. Ravi Acharya*[,§]

Department of Biology and Biochemistry, University of Bath, Claverton Down, Bath BA2 7AY, U.K., and Department de Bioquímica i Biologia Molecular, Facultat de Ciències, Universitat Autònoma de Barcelona, 08193 Bellaterra, Spain

Received July 15, 2002; Revised Manuscript Received August 14, 2002

ABSTRACT: Eosinophil cationic protein (ECP) is a component of the eosinophil granule matrix. It shows marked toxicity against helminth parasites, bacteria single-stranded RNA viruses, and host epithelial cells. Secretion of human ECP is related to eosinophil-associated allergic, asthmatic, and inflammatory diseases. ECP belongs to the pancreatic ribonuclease superfamily of proteins, and the crystal structure of ECP in the unliganded form (determined previously) exhibited a conserved RNase A fold [Boix, E., et al. (1999) *Biochemistry 38*, 16794−16801]. We have now determined a high-resolution (2.0 Å) crystal structure of ECP in complex with adenosine 2′,5′-diphosphate (2′,5′-ADP) which has revealed the details of the ribonucleolytic active site. Residues Gln-14, His-15, and Lys-38 make hydrogen bond interactions with the phosphate at the P_1 site, while His-128 interacts with the purine ring at the B_2 site. A new phosphate binding site, P_{-1}, has been identified which involves Arg-34. This study is the first detailed structural analysis of the nucleotide recognition site in ECP and provides a starting point for the understanding of its substrate specificity and low catalytic efficiency compared with that of the eosinophil-derived neurotoxin (EDN), a close homologue.

Eosinophils secrete cytotoxic granule proteins, cytokines, and lipid mediators, which when they enter the tissue cause allergic and asthmatic diseases (*1*, *2*). The eosinophil granule primarily contains several multifunctional proteins (*3*, *4*) such as eosinophil cationic protein (ECP),[1] eosinophil-derived neurotoxin (EDN), eosinophil major basic protein (EMBP), and eosinophil peroxidase (EPO). ECP and EDN belong to the ribonuclease A (RNase A, EC 3.1.27.5) superfamily of proteins and are also known as RNase 3 and RNase 2, respectively (*5*, *6*). Both these proteins, when injected into either rabbits or guinea pigs, cause the neurotoxic Gordon phenomenon (characterized by muscle stiffness, ataxia, incoordination, and spasmodic paralysis) through the loss of cerebellar Purkinje cells (*7*−*9*). ECP is involved in the immune response system and has marked toxicity for a variety of helminth parasites, hemoflagellates, bacteria, single-stranded RNA viruses, and the host tissues (*10*). Serum ECP levels can be used as a clinical tool for the quantitative estimate of inflammatory activity in asthma and other allergic diseases, and it is related to the severity of the diseases. The antibacterial activity and parasitic toxicity of ECP are higher than those of EDN (*11*, *12*). In vitro, ECP can function as an antiviral agent and may participate in the host defense mechanism against single-stranded RNA respiratory syncytial virus (*13*). The toxicity of ECP against bacteria and helminths does not seem to be related to its RNase activity (*11*, *14*), while the RNase activity of ECP is required for its antiviral (*13*) and neurotoxic activity (*9*). The RNase activity of ECP is known to be ∼100 times lower than that of EDN for most common RNA substrates, and the in vivo substrates of both these enzymes are yet to be identified.

Mature ECP is a small cationic polypeptide of 133 residues, and its molecular mass varies from 16 to 22 kDa due to differences in glycosylation. The amino acid sequence of ECP is 67% identical to that of EDN and 32% to that of RNase A. ECP adopts the kidney-shaped RNase A fold, conserved among all known pancreatic RNase family members (*15*). ECP also possesses the four disulfide bonds and catalytic residues conserved between EDN and RNase A. However, ECP and EDN show significant differences at the secondary substrate binding sites (*16*, *17*). Also, ECP does not possess the C-mannosylation site found at the N-terminus of EDN (EDN's Trp-7-X-X-Trp-10 motif is replaced with an Arg-7-X-X-Trp-10 motif in ECP) (*18*).

A considerable number of studies on RNase A show multiple binding subsite interactions with RNA. These studies have established the presence of subsites designated as B_0−B_n, R_0−R_n, and P_0−P_n, involved in the recognition of base, ribose, and phosphate moieties of the RNA substrate (*19*−*21*). In addition to the main active site (P_1), other phosphate-

[†] This work was supported by Medical Research Council (U.K.) Program Grant 9540039, a Royal Society-Leverhulme Trust (U.K.) Senior Research Fellowship to K.R.A., and Grants BMC2000-0138-C02-01 from Ministerio de Educacion y Cultura and 2000SGR 00064 from CIRIT, Generalitat de Catalunya (Spain), to M.V.N. and C.M.C.

[‡] The atomic coordinates of the ECP−2′,5′-ADP complex have been deposited with the RCSB Protein Data Bank (entry 1H1H).

* To whom correspondence should be addressed. Phone: +44-1225-386 238. Fax: +44-1225-386 779. E-mail: K. R.Acharya@bath.ac.uk.

[§] University of Bath.

[||] Universitat Autònoma de Barcelona.

[1] Abbreviations: ECP, eosinophil cationic protein; EDN, eosinophil-derived neurotoxin; 2′,5′-ADP, adenosine 2′,5′-diphosphate; 3′,5′-ADP, adenosine 3′,5′-diphosphate; 5′-ADP, adenosine 5′-diphosphate.

10.1021/bi0264521 CCC: $22.00
Published on Web 09/12/2002

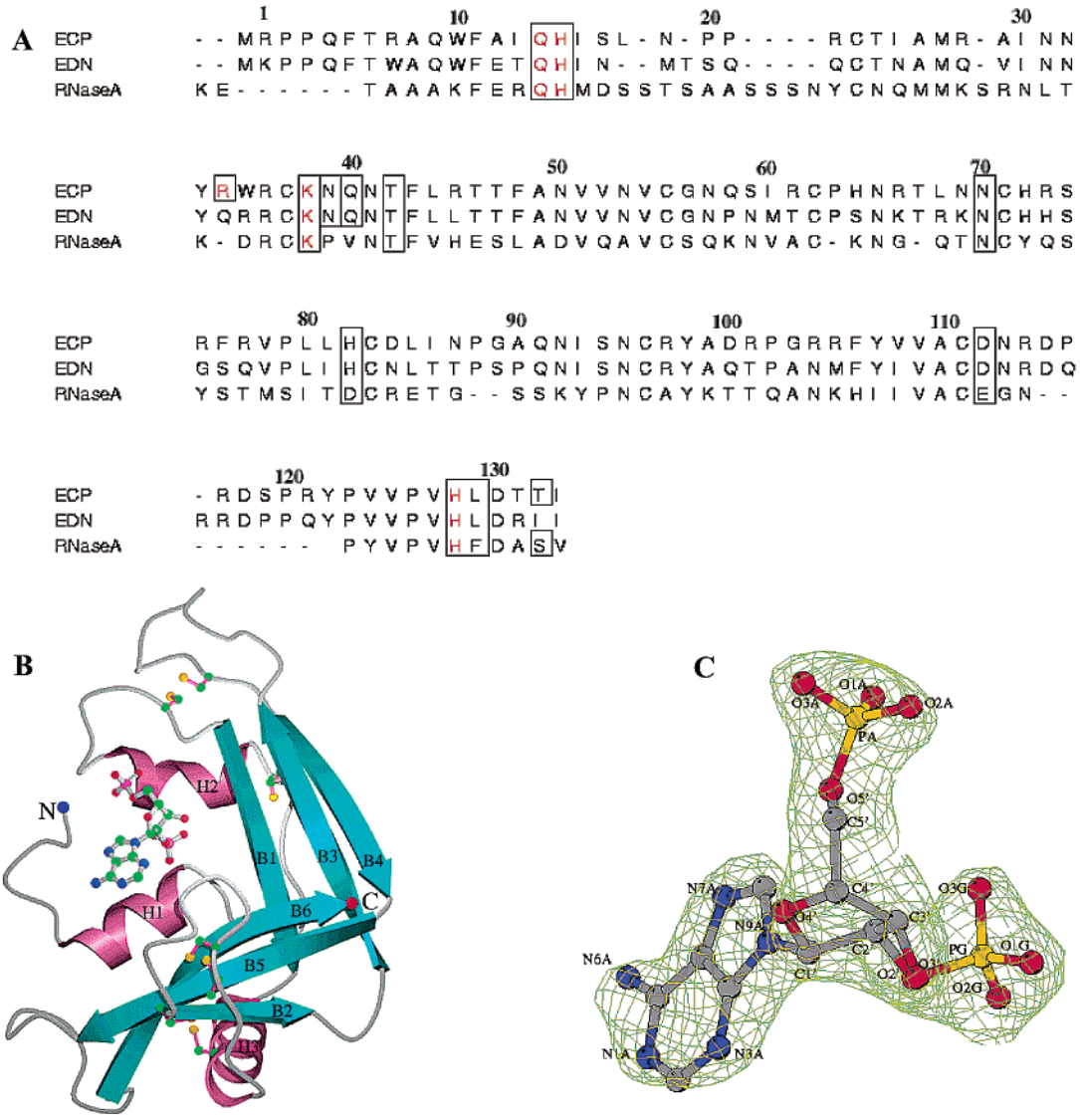

FIGURE 1: (A) Structure-based sequence alignment of ECP, EDN, and RNase A as drawn using ALSCRIPT (*47*). Every tenth residue in the ECP sequence is numbered. Residues that interact with 2′,5′-ADP in ECP are marked in red. Also, conserved residues related to nucleotide binding in RNase A, EDN, and ECP are boxed. (B) Schematic diagram of ECP in complex with 2′,5′-ADP. The 2′,5′-ADP nucleotide is drawn as a ball-and-stick model. This figure was created with BOBSCRIPT (*48*). (C) Diagram of the 2.0 Å sigmaA $2|F_o| - |F_c|$ electron density map of the ECP-bound 2′,5′-ADP nucleotide contoured at the 1.0σ level. The atomic numbering scheme is in accordance with the IUPAC−IUB nomenclature.

binding subsites have been identified, which included P_2, P_0, and P_{-1}. The P_2 site binds the 3′-phosphate of the nucleotide with the base bound at B_2 and the P_0 site the 5′-phosphate of the nucleotide with the base bound at B_1 (*21*−*23*), and the P_{-1} site is adjacent to the P_0 site at the 5′-side (*22*, *24*). A new P_{-1} subsite has been proposed on the basis of the EDN−sulfate complex structure (*25*). On the basis of structural analyses (*17*), a similar site was also proposed for ECP, albeit distinct from the P_{-1} subsite described for RNase A (*22*).

Comparison of the crystal structure of ECP (*17*) with those of EDN and RNase A shows three main catalytic residues at the P_1 subsite which are conserved in all RNase A homologues. In RNase A, these are His-12, Lys-41, and His-119 with the equivalent residues being His-15, Lys-38, and His-129 for EDN and His-15, Lys-38, and His-128 for ECP, respectively. The pyrimidine specific B_1 subsite and the purine-preferring B_2 subsite are partially conserved among RNase A, EDN, and ECP. The B_1 subsite residues in RNase A (Thr-45, Phe-120, and Ser-123) are present in EDN as Thr-42 and Leu-130, and in ECP as Thr-42, Leu-129, and Thr-132, respectively (Figure 1A). The B_2 subsite of RNase A, which includes His-119, Asn-71, and Glu-111, is partially conserved in EDN and ECP as His-129 (His-128), Asn-70, and Asp-112, respectively (Figure 1A) (*16*, *17*, *21*).

Here we present the crystal structure of ECP in complex with 2′,5′-ADP at 2.0 Å resolution. Three different mononucleotides (2′,5′-ADP, 3′,5′-ADP, and 5′-ADP) were examined in this study, of which only 2′,5′-ADP bound to the active site of ECP. This is in contrast to EDN where all three nucleotides bind at the active site as observed from their crystal structures (*16*). This study on ECP has provided details about the interaction of the ribonucleolytic active site residues Gln-14, Lys-38, His-15, and His-128, and some additional information about the ECP substrate specificity. Mainly, the adenine base binds at the B_2 subsite (involving His-128) in ECP, and Arg-34 makes a hydrogen bonding

Table 1: Data Collection and Refinement Statistics

	2′,5′-ADP	3′,5′-ADP	5′-ADP
diffraction data			
resolution (Å)	2.00	2.20	2.85
no. of measured reflections	61821	48691	19440
no. of unique reflections	12663	8405	4351
completeness (%) (outermost shell)[a]	99.4 (99.9)	90.6 (89.8)	99.1 (99.5)
R_{symm} (%)[b]	7.8	9.6	11.4
space group[c]	$P6_3$	$P6_3$	$P6_3$
cell dimensions			
$a = b$ (Å)	100.7	100.1	100.2
c (Å)	31.7	31.2	31.4
$I/\sigma(I)$	14.7	12.2	9.5
refinement statistics			
resolution range (Å)	40−2.0	40−2.20	40−2.85
no. of protein atoms	1102	1102	1102
no. of water molecules	54	45	17
R_{cryst} (%)[d]	20.5	21.1	19.7
R_{free} (%)[e]	21.0	23.4	25.2
rmsd for bond lengths (Å)	0.006	0.007	0.007
rmsd for bond angles (deg)	1.2	1.3	1.3
av *B*-factor for protein atoms (Å^2)	41.5	42.0	45.0
av *B*-factor for nucleotide atoms (Å^2)	56.1	not bound	not bound

[a] The outermost shell is 2.10−2.00, 2.28−2.20, and 2.95−2.85 Å, respectively. [b] $R_{symm} = \sum_h\sum_i|I(h) - I_i(h)|/\sum_h\sum_i I_i(h)$, where $I_i(h)$ and $I(h)$ are the ith and mean measurements of the intensity of reflection h, respectively. [c] One molecule per asymmetric unit. [d] $R_{cryst} = \sum_h|F_o - F_c|/\sum_h F_o$, where F_o and F_c are the observed and calculated structure factor amplitudes of reflection h, respectively. [e] R_{free} is equal to R_{cryst} for a randomly selected 5% subset of reflections not used in the refinement (*30*).

interaction with the 5′-phosphate group in the ECP−2′,5′-ADP complex, forming a putative P_{-1} site.

EXPERIMENTAL PROCEDURES

Materials. Adenosine 2′,5′-diphosphate (2′,5′-ADP), adenosine 3′,5′-diphosphate (3′,5′-ADP), and adenosine 5′-diphosphate (5′-ADP) were purchased from Sigma. Uridylyl-3′,5′-adenosine (UpA) was purchased from ICN Biochemicals.

Crystallization, Data Collection, and Refinement. Recombinant ECP was expressed in *Escherichia coli* and purified as described previously (*26*). Hexagonal crystals of ECP were grown as described by Boix et al. (*17*). Native ECP crystals were soaked for 48 h prior to data collection with either 25 mM 2′,5′-ADP, 3′,5′-ADP, or 5′-ADP dissolved in crystallization buffer [0.5 M NaCl, 10% 2-propanol, and 0.1 M HEPES-NaOH (pH 8.0)]. A single crystal was used to collect data for each soaking experiment. The ECP crystals soaked with 2′,5′-ADP diffracted to 2.0 Å resolution on the Synchrotron Radiation Source at Daresbury (Warrington, U.K.) (station PX 9.6), and the data were acquired using an ADSC Quantum 4 CCD detector system. Data for the ECP crystal soaked with 3′,5′-ADP were collected on station PX 14.2 to a resolution of 2.2 Å and for 5′-ADP on station PX 14.1 to a resolution of 2.85 Å. All data sets were collected at room temperature. Using DENZO (*27*), all raw data images were first indexed, integrated, and corrected for Lorentz and polarization effects. Data were scaled and merged using SCALEPACK (*27*). Intensities were further truncated to amplitudes using TRUNCATE (*28*). Details of data collection and processing statistics are presented in Table 1.

The refinement of the structures was carried out using CNS (*29*) with the native structure of ECP (*17*) as a starting model. Several alternating cycles of refinement, energy minimization, individual temperature factor refinement, simulated annealing, and model building were performed until the R_{free} (*30*) value could not be further improved. Water molecules were then gradually inserted into the model at positions corresponding to peaks in the $|F_o| - |F_c|$ electron density map with heights greater than 3σ and at hydrogen bond forming distances from appropriate atoms. Water molecules with temperature factors of >65 Å^2 were excluded from subsequent refinement steps. The nucleotide molecule was included in the final stages of CNS refinement. The details of the refinement statistics are presented in Table 1. The program PROCHECK (*31*) was used to analyze the quality of the final structure. Analysis of the Ramachandran ($\phi-\psi$) plot for the structure showed that all residues lie in the allowed regions.

Kinetic Analysis of ECP. RNase activity of ECP was measured by a spectrophotometric method. Assays were carried out at 25 °C in 0.1 M MES (pH 6.0) and 0.1 M HEPES buffer (pH 8.0) using a 0.5 cm path length cell. UpA was used as a substrate. Substrate and inhibitor concentrations were determined spectrophotometrically using the following extinction coefficients: $\epsilon_{261} = 23\,500$ M^{-1} cm^{-1} for UpA (*32*) and $\epsilon_{259} = 15\,400$ M^{-1} cm^{-1} for 5′-ADP, 2′,5′-ADP, and 3′,5′-ADP (*33*). The activity was measured by following the initial reaction velocities using the difference molar absorbance coefficient ($\Delta\epsilon_{286} = 570$ M^{-1} cm^{-1}) for the transphosphorylation reaction of UpA (*34*). K_i values were determined by the Dixon method (*35*) using concentrations of 0.15 and 0.3 mM UpA, and five inhibitor concentrations from 0.0 to 0.2 mM; $1/v_0$ (where v_0 is the initial velocity) was plotted against the inhibitor concentration, [I] (data not shown).

RESULTS AND DISCUSSION

The structure of ECP in complex with 2′,5′-ADP is shown in Figure 1B. The root-mean-square deviation of the C^α atoms of the native ECP (*17*) and the present ECP−2′,5′-ADP complex structure is 0.31 Å. Fifty-four water molecules were identified in the structure of the ECP−2′,5′-ADP complex. The active site residues in ECP show no significant conformational change upon nucleotide binding.

The side chain of RNase A, His-119, and its EDN counterpart, His-129, are highly mobile and tend to adopt one of two main conformations (A and B), with a χ_1 of $\approx$150° and a χ_2 of $\approx$60° (*36*, *37*). In the RNase A structure, conformation A was identified as the catalytically active conformation (*38*, *39*) and is found to be compatible with substrate binding (*16*, *39*). A similar active conformation has been observed for His-129 in EDN and in complex with 3′,5′-ADP, while in the EDN−2′,5′-ADP and EDN−5′-ADP complexes, this His residue adopts the B conformation (*16*). Residue His-128 in ECP (in both the native and complex structures) adopts conformation A, with a χ_1 of 179°. However, in the ECP structure determined by Mallorquí-Fernández et al. (*40*), His-128 adopted an inactive conformation (conformation B), and this could be attributed to the difference in the crystallization conditions and crystal packing.

Table 2: Comparison of Torsion Angles of 2′,5′-ADP When It Is Bound to ECP (this study) or EDN (*16*)[a]

	ECP	EDN
backbone torsion angle (deg)		
O5′−C5′−C4′−C3′ (γ)	69 (+*sc*)	59 (+*sc*)
C5′−C4′−C3′−O3′ (δ)	139 (+*ac*)	158 (*ap*)
C5′−C4′−C3′−C2′	−96	−85
C4′−C3′−C2′−O2′	−160	−162
glycosyl torsion angle (deg)		
O4′−C1′−N9A−C4A (χ)	−112 (*anti*)	−91 (*anti*)
pseudorotation angle (deg)		
C4′−O4′−C1′−C2′ (ν_0)	−26	−12
O4′−C1′−C2′−C3′ (ν_1)	42	33
C1′−C2′−C3′−C4′ (ν_2)	−41	−40
C2′−C3′−C4′−O4′ (ν_3)	25	34
C3′−C4′−O4′−C1′ (ν_4)	0	−14
phase (deg)	C2′-*endo*	C2′-*endo*
phosphate torsion angle (deg)		
O3A−PA−O5′−C5′ (α)	−	−
PA−O5′−C5′−C4′ (β)	−156 (*ap*)	−168 (*ap*)

[a] Torsion angles are defined in accordance with the IUPAC−IUB nomenclature (*46*).

Table 3: Hydrogen Bonding Interactions of ECP (this study) and EDN (*16*) with 2′,5′-ADP

			distance (Å)	
ECP	EDN[a]	2′,5′-ADP[b]	ECP	EDN
Gln-14 Nϵ2	Gln-14 Nϵ2	O1G	3.0	3.3
His-15 Nϵ2	His-15 Nϵ2	O3G	3.0	2.6
Arg-34 Nϵ2		O2A	2.7	−
Lys-38 Nζ		O2G	2.8	−
His-128 Nϵ2		N3A	3.3	−
	His-129 Nϵ2	O1G	−	2.7
	Leu-130 N	O3G	−	2.8
water[c]		O3G	2.4	2.8
water		O3G	3.1	−
water		O2A	2.7	−
water		O1A	2.7	2.9
water		O1G	3.1	−
symmetry-related hydrogen bonding contacts				
Gln-4 Nϵ2		O3A	3.1	−
Asn-32 O		N6A	2.9	−
Tyr-33 OH		O3A	3.2	−

[a] EDN−2′,5′-ADP complex (PDB entry 1HI3) (*16*). [b] Atom numbering for 2′,5′-ADP is defined according to Figure 1C. [c] For the EDN complex, conserved waters are considered.

Binding of 2′,5′-ADP to ECP. The structure of 2′,5′-ADP is well-defined in the electron density map (Figure 1C). When bound to ECP, the deoxyribose moiety of 2′,5′-ADP adopts the energetically favorable C2′-*endo* anti conformation and a γ torsion angle of 69° (Table 2) which is in the synclinal range (+*sc*), usually found in free nucleotides (*41*). A stereoview of the binding of 2′,5′-ADP to ECP is shown in Figure 2.

The rms deviation between the C$^\alpha$ atoms of the superimposed ECP−2′,5′-ADP and EDN−2′,5′-ADP structures is 0.99 Å, and the rms deviations between ECP and the EDN−3′,5′-ADP and EDN−5′-ADP structures are 1.1 and 1.0 Å, respectively. The superimposed structures of the ECP−2′,5′-ADP and EDN−2′,5′-ADP complexes, native ECP with the EDN−3′,5′-ADP complex, and native ECP with the EDN−5′-ADP complex are shown in panels A−C of Figure 3, respectively. These show differences in the degree of conformational freedom at the ribonucleolytic active site residues for the adenylic diphosphate nucleotides (2′,5′-ADP, 3′,5′-ADP, and 5′-ADP) in ECP and EDN.

The mode of binding of 2′,5′-ADP to ECP and EDN is similar. In both cases, the backbone torsion angles (γ) are in +*sc* range (Table 2). The torsion angle (δ) of the 2′,5′-ADP−ECP complex is anticlinal (+*ac*; 139°), while that of the 2′,5′-ADP−EDN complex is antiperiplanar (*ap*; 158°). The other backbone torsion angles are very similar in both cases. Glycosidic torsion angles (χ) of the nucleotide in both ECP and EDN nucleotide complexes differ by 20°, and both are in the *anti* conformation. The pseudorotation angles ν_0−ν_3 are broadly conserved, and also the 5′-phosphate torsion angle (β) is maintained in the *ap* range (Table 2).

The binding of 2′,5′-ADP to ECP is mainly at the active site P_1−B_2 region (Figure 2). In the ECP−2′,5′-ADP complex, the 2′-phosphate occupies the P_1 site and forms a set of hydrogen bonds with the side chains of Gln-14, His-15, and Lys-38 (Table 3 and Figure 2). Similar hydrogen bonding contacts have been observed in the case of the EDN−2′,5′-ADP complex (Figure 3A and Table 3). In addition, a weak hydrogen bond contact between His-128 and the nucleotide base is observed in the ECP−2′,5′-ADP complex (Table 3 and Figure 2) which is absent in the EDN−2′,5′-ADP complex. In the ECP−2′,5′-ADP complex, the adenine ring is not parallel to the imidazole ring of His-128 (Figure 2), but in the case of the EDN−2′,5′-ADP complex, the adenine ring adopts a conformation which is almost parallel to the imidazole ring of His-129. Interestingly, in

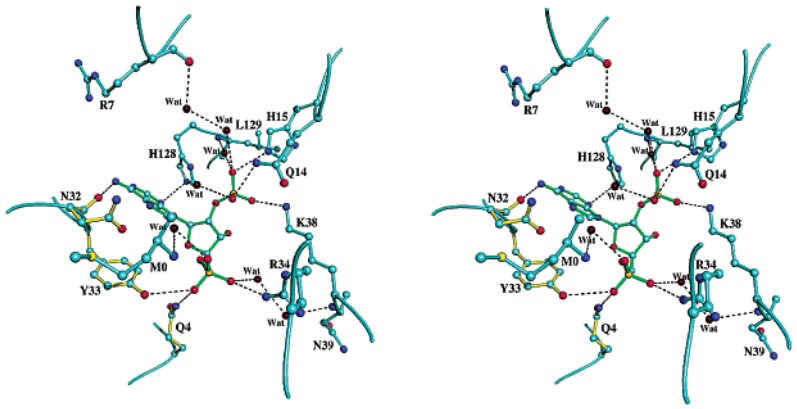

FIGURE 2: Stereoview showing the interaction of 2′,5′-ADP with ECP. Water-mediated hydrogen bonding interactions are also shown. ECP residues and the nucleotide molecule are shown in cyan with oxygen atoms in red and nitrogen atoms in blue; water molecules are depicted as brown spheres. The symmetry-related contact residues are shown in yellow. Hydrogen bonds are shown as dashed lines.

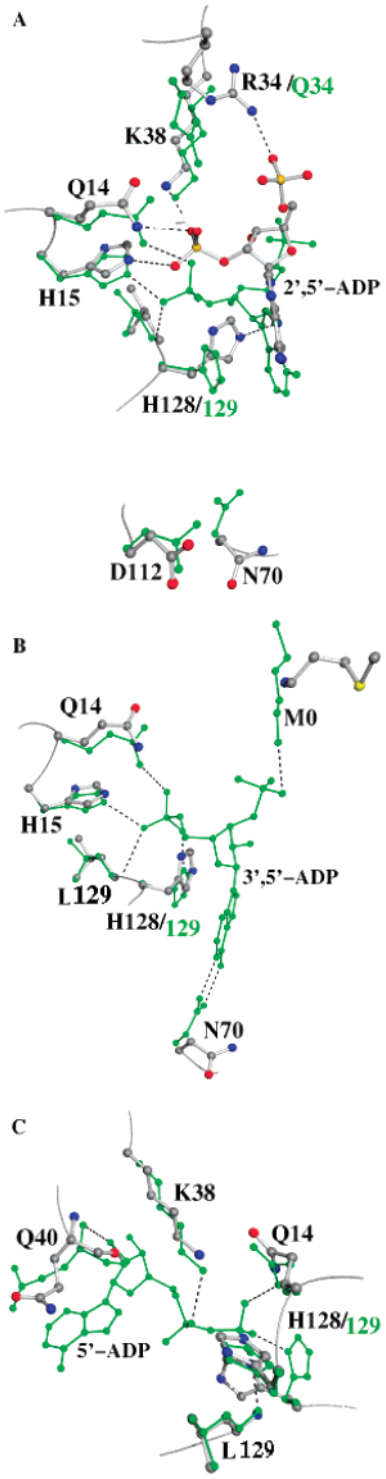

FIGURE 3: Superimposed structures of (A) the ECP−2′,5′-ADP and EDN−2′,5′-ADP complexes (PDB entry 1HI3) as well as those of ECP (PDB entry 1QMT) with EDN nucleotide complexes [(B) 3′,5′-ADP and (C) 5′-ADP (PDB entries 1HI4 and 1HI5, respectively) (*16*)]. The amino acid residues for the ECP−2′,5′-ADP complex are gray, and those of EDN−nucleotide complexes are green. Oxygen and nitrogen atoms are red and blue, respectively, for the ECP−2′,5′-ADP structure. Hydrogen bonds are shown as dashed lines.

both the ECP−2′,5′-ADP and EDN−3′,5′-ADP complexes, the imidazole ring of His-128 (His-129 in EDN) adopts conformation A, but in the EDN−2′,5′-ADP complex, the imidazole ring of His-129 adopts conformation B.

A novel P_{-1} subsite region was identified in ECP and EDN, located upstream of the cleavable phosphodiester bond (*17*, *25*). The 5′-phosphate group of 2′,5′-ADP makes a hydrogen bond interaction with the side chain of Arg-34, which is part of this P_{-1} subsite. The 5′-phosphate group also makes hydrogen bonding interactions with symmetry-related Gln-4 and Tyr-33 residues. The binding of the 5′-phosphate group in the ECP−2′,5′-ADP complex takes place in a specific orientation different from that expected from the RNase A binding subsite model where it would be expected to bind at the P_2 subsite. In contrast, in the EDN−2′,5′-ADP complex, the 5′-phosphate group is not involved in hydrogen bonding interactions with EDN or symmetry-related molecules. In addition, the main chain of a symmetry-related Asn-32 residue makes a hydrogen bonding interaction with the amino group of the purine ring in the ECP−2′,5′-ADP complex (Figure 2 and Table 3). The packing interactions involving residues Gln-4, Asn-32, and Tyr-33 are nevertheless conserved between native ECP and EDN. Shifts in the orientations of residues Asn-70 and Asp-112 (which correspond to the B_2 subsite) are observed in the ECP−2′,5′-ADP complex when compared to their EDN−2′,5′-ADP counterparts, although in both cases the corresponding residues do not interact directly with the nucleotide, as only observed for Asn-70 in the EDN−3′,5′-ADP complex (Figure 3A,B). The lower substrate affinity and catalytic efficiency of ECP might be due to an impaired B_2 binding subsite together with the absence of the P_2 subsite (*17*, *26*).

There are also some differences in the hydrogen bonding interactions of ECP and EDN with 2′,5′-ADP. In the EDN−2′,5′-ADP complex, there exists a hydrogen bond between Leu-130 and the 2′-phosphate group of 2′,5′-ADP (*16*), which is not found in the present ECP−2′,5′-ADP complex structure. In ECP, Asp-112 and Arg-7 make strong hydrogen bonding interactions between the Nϵ2 atom of Arg-7 and the Oδ2 atom of Asp-112. This feature is not observed in EDN, but the corresponding residue in EDN (Trp-7) does make van der Waals interactions with the 3′,5′-ADP and 5′-ADP nucleotide (*16*). The other feature observed in both the ECP and EDN complexes is that the main chain oxygen atom of Trp-10 makes a hydrogen bond with the main chain of Gln-14. There is a major structural rearrangement at the loop region from Asn-32 to Arg-36 due to variation in the primary sequence of ECP and EDN. This is significant since the P_{-1} subsite residue is located in this region in both the ECP and EDN molecules.

There are five water molecules making direct hydrogen bonding interactions with the 2′- and 5′-phosphates of the nucleotide in the ECP−2′,5′-ADP complex (Figure 2 and Table 3). Furthermore, both ECP and 2′,5′-ADP participate in an extended water-mediated hydrogen bonding network involving six water molecules, the side chains of residues Arg-7, Gln-14, Arg-34, and Asn-39, and the main chain of Leu-129 (Figure 2). The nucleotide is also involved in water-mediated interactions with the α-amino group of Met-0 at the N-terminus as observed in the EDN−2′,5′-ADP complex. In addition, 2′,5′-ADP in the ECP complex also makes van der Waals interactions with the side chains of Met-0 and Asn-41.

The main catalytic residues required for RNase activity are conserved in ECP, as in all other members of the mammalian RNase family. Site-directed mutagenesis of two

of these residues, Lys-38 to arginine and His-128 to aspartate, eliminates the RNase activity of ECP (*11*). Another important fact is that the weakening of the His-128−Asp-130 interaction in eosinophil RNases may explain the reduction in activity and the lower pH range for the optimum activity of its transphosphorylation reaction (*15*). In RNase A, the corresponding His-119−Asp-121 catalytic dyad does play an important role in this reaction (*19*). The histidine−aspartic acid catalytic dyad could contribute for the respective RNase activities in RNase A, EDN, and ECP. Interestingly, from the crystal structure analysis, this interaction is found to be stronger (based on the distance) in RNase A (2.6 Å) than in EDN (2.8 Å), and no interaction is observed in ECP (4.6 Å).

Several orthologs of ECP have been identified and characterized enzymatically. All of them maintain the classic catalytic triad (His-15, Lys-38, and His-128) and have the conserved Gln-14 residue. Also, an evolutionary analysis of the single sequence homologue of ECP and/or EDN in the primate ribonuclease gene family has been carried out by Rosenberg et al. (*42*). The results of this analysis have clearly suggested two novel functions: increased cationicity and/or toxicity (ECP) and enhanced ribonuclease activity (EDN) arising due to evolutionary constraints (*43*). However, the relative catalytic efficiency of these ECP orthologs, and that of the single sequence of EDN and/or ECP found among the New World monkey species, could not be predicted with the available crystallographic and kinetic data.

Lack of Binding of 3′,5′-ADP and 5′-ADP to Crystalline ECP. We have repeatedly tested the binding of 3′,5′-ADP and 5′-ADP nucleotides to ECP (by cocrystallization and soaking methods), but no binding was observed in the crystal. A simple modeling exercise in which the 3′,5′-ADP and 5′-ADP nucleotides from the respective EDN complexes are superimposed on the active site of ECP shows distinct steric clashes (Figure 3B,C). His-128 and Trp-35 (symmetry-related molecule) from ECP are directly involved in these clashes.

Docking analysis was also performed using the AUTODOCK program (*44*) to check the nucleotide binding ability to the enzyme. Among the three nucleotides that were studied here, none of them predicted the required conformational arrangement (or the mode of binding) for making the hydrogen bonding interactions with the enzyme.

Inhibition of ECP Enzymatic Activity by 2′,5′-ADP, 3′,5′-ADP, and 5′-ADP. The inhibition constants for these adenylic nucleotides have been determined spectrophotometrically. Kinetic assays were initially carried out at pH 8.0, the pH used for the crystallization buffer to grow ECP crystals. However, the kinetic analysis at pH 8.0 with the spectrophotometric assay did not allow the determination of the K_i value as the catalytic efficiency of the enzyme was very low and the inhibitor−enzyme interactions very weak; therefore, a detailed kinetic analysis was performed at pH 6.0 to increase the affinity of the inhibitor for the enzyme. The estimated K_i values at pH 6.0 obtained from the study presented here and obtained using the Dixon plot analysis are in the range of 2−3 μM for 5′-ADP and 6−7 μM for 2′,5′-ADP and 3′,5′-ADP. The results indicate that there are no significant differences in the affinity constants between the three assayed adenylic nucleotides. However, our crystallographic data clearly show the binding of only 2′,5′-ADP to ECP in the crystalline state due to steric clashes (see above). Previous kinetic characterization of eosinophil RNases (*15*) reported an activity optimum of ∼6.5. An increased nucleotide affinity should also be expected at an even lower pH, as described for RNase A (*45*). Therefore, lower K_i values would be expected for the mononucleotides at pH 6.0 than at pH 8.0. Previous kinetic analyses of EDN have shown that 3′,5′-ADP has a slightly higher binding affinity for EDN (lower K_i value) than 2′,5′-ADP and 5′-ADP (*16*). However, the comparison of the determined K_i values with the reported ones in the literature should take into account the differences in both the pH and ionic strength of the assay mixture.

CONCLUSIONS

Analysis of the crystal structure of the ECP−2′,5′-ADP complex has enabled us to identify for the first time some of the key residues involved in the substrate specificity of ECP, i.e., the P_1, B_2, and P_{-1} subsites. The P_1 subsite is conserved in ECP, EDN, and all pancreatic RNase superfamily members that have been examined. The B_2 subsite of ECP does bind adenine as in RNase A and EDN nucleotide complexes. A P_{-1} subsite has been identified in the ECP−2′,5′-ADP complex presented here, and this site is conserved in EDN but not in RNase A. The molecular basis of RNase activity inhibition has yet to be understood in ECP, particularly in view of its lower substrate affinity and catalytic efficiency. Meanwhile, further analysis of ECP−nucleotide complexes which are currently in progress might prove to be useful for the design of inhibitors.

ACKNOWLEDGMENT

We are grateful to the staff at the Synchrotron Radiation Source, Daresbury, for their help with X-ray data collection. We also thank members of the Structural Biology Group at Bath, in particular Daniel E. Holloway for the constructive criticisms of the manuscript.

REFERENCES

1. Ackerman, S. J. (1993) in *Eosinophils: Biological and Clinical Aspects* (Makino, S., and Fukuda, T., Eds.) pp 33−74, CRC Press, Boca Raton, FL.
2. Snyder, M. R., and Gleich, G. J. (1997) in *Ribonucleases: Structures and Functions* (D'Alessio, G., and Riordan, J. F., Eds.) pp 425−444, Academic Press, New York.
3. Gleich, G. J. (1996) *Allergol. Int. 45*, 35−44.
4. Rosenberg, H. F., Tenen, D. G., and Ackerman, S. J. (1989) *Proc. Natl. Acad. Sci. U.S.A. 86*, 4460−4464.
5. Boix, E. (2001) *Methods Enzymol. 341*, 287−305.
6. Rosenberg, H. F., and Domachowske, J. B. (2001) *Methods Enzymol. 341*, 273−286.
7. Gleich, G. J., and Adolphson, C. R. (1986) *Adv. Immunol. 39*, 177−253.
8. Fredens, K., Dahl, R., and Venge, P. (1982) *J. Allergy Clin. Immunol. 70*, 361−366.
9. Sorrentino, S., Glitz, D. G., Hamann, K. J., Loegering, D. A., Checkel, J. L., and Gleich, G. J. (1992) *J. Biol. Chem. 267*, 14859−14865.
10. Gleich, G. J., Adolphson, C. R., and Leiferman, K. M. (1993) *Annu. Rev. Med. 44*, 85−101.
11. Rosenberg, H. F. (1995) *J. Biol. Chem. 270*, 7876−7881.
12. Rosenberg, H. F. (1998) *Cell. Mol. Life Sci. 54*, 795−803.
13. Domachowske, J. B., Dyer, K. D., Adams, A. G., Leto, T. L., and Rosenberg, H. F. (1998) *Nucleic Acids Res. 26*, 3358−3363.
14. Lehrer, R. I., Szklarek, D., Barton, A., Ganz, T., Hamann, K. J., and Gleich, G. J. (1989) *J. Immunol. 142*, 4428−4434.
15. Sorrentino, S., and Libonati, M. (1994) *Arch. Biochem. Biophys. 312*, 340−348.

16. Leonidas, D. D., Boix, E., Prill, R., Suzuki, M., Turton, R., Minson, K., Swaminathan, G. J., Youle, R. J., and Acharya, K. R. (2001) *J. Biol. Chem. 276*, 15009−15017.
17. Boix, E., Leonidas, D. D., Nikolovski, Z., Nogués, M. V., Cuchillo, C. M., and Acharya, K. R. (1999) *Biochemistry 38*, 16794−16801.
18. Krieg, J., Hartmann, S., Vicentini, A., Glasner, W., Hess, D., and Hofsteenge, J. (1998) *Mol. Biol. Cell 9*, 301−309.
19. Richards, F. M., and Wyckoff, H. W. (1971) in *The Enzymes* (Boyer, P. D., Ed.) pp 647−806, Academic Press, New York.
20. Pares, X., Nogués, M. V., de Llorens, R., and Cuchillo, C. M. (1991) *Essays Biochem. 26*, 89−103.
21. Cuchillo, C. M., Vilanova, M., and Nogués, M. (1997) in *Ribonucleases: Structure and Function*, Academic Press, New York.
22. Fisher, B. M., Grilley, J. E., and Raines, R. T. (1998) *J. Biol. Chem. 273*, 34134−34138.
23. Nogués, M. V., Moussaoui, M., Boix, E., Vilanova, M., Ribo, M., and Cuchillo, C. M. (1998) *Cell. Mol. Life Sci. 54*, 766−774.
24. Fontecilla-Camps, J. C., de Llorens, R., le Du, M. H., and Cuchillo, C. M. (1994) *J. Biol. Chem. 269*, 21526−21531.
25. Mosimann, S. C., Newton, D. L., Youle, R. J., and James, M. N. (1996) *J. Mol. Biol. 260*, 540−552.
26. Boix, E., Nikolovski, Z., Moiseyev, G. P., Rosenberg, H. F., Cuchillo, C. M., and Nogués, M. V. (1999) *J. Biol. Chem. 274*, 15605−15614.
27. Otowinowski, Z., and Minor, W. (1997) *Methods in Enzymology*, Vol. 276, Academic Press, New York.
28. French, S., and Wilson, K. S. (1978) *Acta Crystallogr. A34*, 517−525.
29. Brünger, A. T., Adams, P. D., Clore, G. M., DeLano, W. L., Gros, P., Grosse-Kunstleve, R. W., Jiang, J. S., Kuszewski, J., Nilges, M., Pannu, N. S., Read, R. J., Rice, L. M., Simonson, T., and Warren, G. L. (1998) *Acta Crystallogr. D54*, 905−921.
30. Brünger, A. T. (1992) *Nature 355*, 472−475.
31. Laskowski, R. A., MacArthur, M. W., Moss, D. S., and Thornton, J. M. (1993) *J. Appl. Crystallogr. 26*, 283−291.
32. Imazawa, M., Irie, M., and Ukita, T. (1968) *J. Biochem. 64*, 595−602.
33. Sambrook, J., Fritsch, E. F., and Maniatis, T. (1989) *Molecular Cloning: A Laboratory Manual*, Cold Spring Harbor Laboratory Press, Plainview, NY.
34. Moiseev, G. P., Bocharov, A. L., Mamaeva, O. K., and Yakolev, G. J. (1982) *Bioorg. Khim. 8*, 1197−1206.
35. Dixon, M. (1953) *Biochem. J. 55*, 170−171.
36. Swaminathan, G. J., Holloway, D. E., Veluraja, K., and Acharya, K. R. (2002) *Biochemistry 41*, 3341−3352.
37. Zegers, I., Maes, D., Dao-Thi, M. H., Poortmans, F., Palmer, R., and Wyns, L. (1994) *Protein Sci. 3*, 2322−2339.
38. Borkakoti, N. (1983) *Eur. J. Biochem. 132*, 89−94.
39. Leonidas, D. D., Shapiro, R., Irons, L. I., Russo, N., and Acharya, K. R. (1997) *Biochemistry 36*, 5578−5588.
40. Mallorquí-Fernández, G., Pous, J., Peracaula, R., Aymamí, J., Maeda, T., Tada, H., Yamada, H., Seno, M., de Llorens, R., Gomis-Rüth, F. X., and Coll, M. (2000) *J. Mol. Biol. 300*, 1297−1307.
41. Moodie, S. L., and Thornton, J. M. (1993) *Nucleic Acids Res. 21*, 1369−1380.
42. Rosenberg, H. F., Dyer, K. D., Tiffany, H. L., and Gonzalez, M. (1995) *Nat. Genet. 10*, 219−223.
43. Rosenberg, H. F., and Dyer, K. D. (1995) *J. Biol. Chem. 270*, 21539−21544.
44. Morris, G. M., Goodsell, D. S., Halliday, R. S., Huey, R., Hart, W. E., Belew, R. K., and Olson, A. J. (1998) *J. Comput. Chem. 19*, 1639−1662.
45. Russo, A., Acharya, K. R., and Shapiro, R. (2001) *Methods Enzymol. 341*, 629−648.
46. IUPAC Commission on Nomenclature of Organic Chemistry Rules for the Nomenclature of Organic Chemistry, Section E: Stereochemistry, Recommendations 1974 (1976) *Pure Appl. Chem. 45*, 11−30.
47. Barton, G. J. (1993) *Protein Eng. 6*, 37−40.
48. Esnouf, R. M. (1999) *Acta Crystallogr. D55*, 938−940.

BI0264521